Chinese Chemical Letters 33 (2022) 2928–2932

Contents lists available at ScienceDirect

Chinese Chemical Letters

journal homepage: www.elsevier.com/locate/cclet

Bimetallic cobalt-nickel coordination polymer electrocatalysts for enhancing oxygen evolution reaction

Lele Lu, Qiang Li, Jia Du, Wei Shi*, Peng Cheng

Department of Chemistry, Key Laboratory of Advanced Energy Materials Chemistry (MOE), Renewable Energy Conversion and Storage Center (RECAST), College of Chemistry, Nankai University, Tianjin 300071, China

ARTICLE INFO

Article history:
Received 30 July 2021
Revised 16 September 2021
Accepted 28 October 2021
Available online 5 November 2021

Keywords:
Coordination polymer
Mixed-metal strategy
Electrocatalysis
Oxygen evolution reaction
Activation energy

ABSTRACT

Coordination polymers (CPs) have great potential to be used in electrocatalysis owing to their designable compositions and structures. It is highly challenging to apply CPs as electrocatalysts for oxygen evolution reaction (OER) on account of insufficient catalytic efficiency and relatively poor stability of current electrocatalysts. Herein, through a mixed-metal strategy, one-dimensional Co_xNi_{1-x}-HIPA with dual active sites was synthesized and studied for OER electrocatalysts. By changing the metal ratio of Co_xNi_{1-x}-HIPA, the OER performance was well regulated. The optimized $Co_{1/2}Ni_{1/2}$-HIPA exhibited minimum reaction activation energy, and represented an overpotential of 367 mV to reach 10 mA/cm^2 at 25 °C. Moreover, an overpotential of 314 mV at 10 mA/cm^2 was obtained from $Co_{1/2}Ni_{1/2}$-HIPA at 55 °C. This mixed-metal strategy provides a feasible way for adjusting the electronic states of the electrocatalysts to improve the electrocatalytic OER performance.

As two main challenges of the 21st century, the everlasting global energy consumption relying mostly on fossil fuels and the consequent climate change are tilting the balance of our society [1–4]. One way out of this dilemma is to resort to the development of sustainable and environmentally friendly energy instead. Among all candidates, hydrogen energy attracts broad interest due to its rich resources, high combustion calorific value and pollution-free feature [5–8]. Electrocatalytic water splitting has been deemed as one of the most promising methods for hydrogen production. Nevertheless, the application of electrocatalytic water splitting is subject to anodic oxygen evolution reaction (OER), which possesses a large thermodynamic equilibrium potential of 1.23 V *vs.* reversible hydrogen electrode (RHE), and involves a multistep proton-coupled 4e$^-$ transfer process [9–11]. Hitherto, representative high-efficiency catalysts for OER are mostly noble metal-based compounds like IrO_2 and RuO_2, yet their restricted resources and high-price stand in the way of large-scale applications [12,13]. To address this complication, enormous efforts have been made to utilize earth-abundant transition metal-based electrocatalysts for the next generation of OER electrocatalysts [14–17].

Coordination polymers (CPs), a type of coordination compounds with long-range ordered and adjustable structures resulting from coordination between metal nodes and organic ligands, have been widely studied for the applications of catalysis, fluorescence, and energy storage [18–26]. The application of CPs in the field of electrocatalysis mainly involves two kinds: (1) using CPs as precursors to fabricate metal-based nanostructures as electrocatalysts through high-temperature calcination [27,28]; (2) directly utilizing CPs with high-activity as electrocatalysts [29–31]. The metal centers of CPs are generally the active sites, therefore the regulation of metal types, coordination environment, defects, *etc.* are crucial to improve their electrocatalytic properties. By introducing different kinds of metals into CPs and adjusting their proportion, it is expected to fabricate highly efficient OER catalysts. However, there are still few related examples referring to electrocatalysts based on bimetallic CPs and the regulation of the metal proportion for enhanced OER performance [32–37].

In this contribution, one-dimensional (1D) bimetallic CPs with formula of $[Co_xNi_{1-x}(HIPA)(H_2O)_3]_n$ (Co_xNi_{1-x}-HIPA, H_3IPA = 5-hydroxyisophthalic acid) are elaborately designed and fabricated with a modified hydrothermal method. The well-designed mixed-metal strategy for the construction of bimetallic CPs with long-range ordered crystal structure and uniform distribution of different metal elements is beneficial for efficient charge density regulation that result in enhanced catalytic activity. The optimal $Co_{1/2}Ni_{1/2}$-HIPA shows the lowest overpotential and the smallest Tafel slope (TS) in alkaline electrolyte. Furthermore, we also explored the effect of temperature on OER activity of CP-based electrocatalysts for the first time. The resulted activation energies of

* Corresponding author.
E-mail address: shiwei@nankai.edu.cn (W. Shi).

https://doi.org/10.1016/j.cclet.2021.10.090
1001-8417/

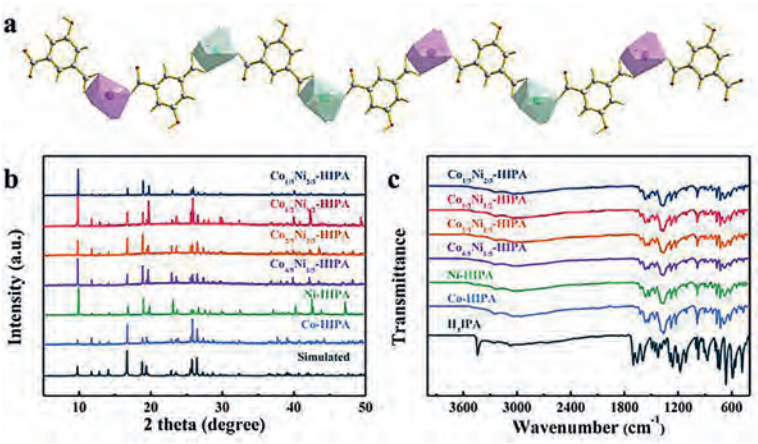

Fig. 1. (a) 1D structure of Co_xNi_{1-x}-HIPA (Co and Ni centers distributed randomly in the Co_xNi_{1-x}-HIPA); (b) PXRD patterns of Co_xNi_{1-x}-HIPA and the simulated diffraction pattern of Co-HIPA; (c) FTIR spectra of Co_xNi_{1-x}-HIPA and H_3IPA.

the catalysts and the electron states confirm that this mixed-metal strategy could ultimately result in enhanced electrocatalysts for oxygen evolution reaction.

The reaction of H_3IPA and different molar ratios of $Co(OAc)_2{\cdot}4H_2O$ and $Ni(OAc)_2{\cdot}4H_2O$ led to the formation of Co_xNi_{1-x}-HIPA (x = 0, 1/3, 1/2, 2/3, 4/5, 1). Based on the single crystal data of Co-HIPA and Ni-HIPA [38], each Co or Ni center is connected to three O atoms from two $HIPA^{2-}$ ligands, and other coordination sites are taken up by three H_2O molecules, forming an octahedral environment. The alternating connection of $HIPA^{2-}$ and metal centers lead to a chain structure (Fig. 1a). Hydrogen bonds between H_2O molecules and the oxygen of ligands connect adjacent chains into a three-dimensional supramolecular framework (Fig. S1 in Supporting information).

According to inductively coupled plasma-optical (ICP) data (Table S1 in Supporting information), the molar ratios of metal centers in Co_xNi_{1-x}-HIPA fit the feeding molar ratios. Powder X-ray diffraction (PXRD) patterns of all Co_xNi_{1-x}-HIPA are identical to the Co/Ni-HIPA (Fig. 1b), which proves their isostructural nature and high phase purity. As shown in Fig. 1c, Fourier transform infrared (FTIR) spectra of all Co_xNi_{1-x}-HIPA are similar as well, further confirming their isomorphism. Thermal gravimetric analysis (TGA) curves display similar weight loss from ~150 °C to 230 °C, which can be attributed to the loss of three coordinated H_2O molecules (Fig. S2 in Supporting information). The collapse of the coordination frameworks occurred over 400 °C.

Scanning electron microscopy (SEM) was applied to examine the morphology of Co_xNi_{1-x}-HIPA. All the Co_xNi_{1-x}-HIPA show the regular rod-like morphology (Fig. S3 in Supporting information). Herein, $Co_{1/2}Ni_{1/2}$-HIPA, which proves to be the best OER electrocatalyst, is chosen for more detailed examination. Both transmission electron microscopy (TEM) and scanning transmission electron microscopy (STEM) images confirm its rod-like morphology (Figs. 2a and b). Energy-dispersive X-ray spectroscopy (EDS) elemental mapping results reveal that Co, Ni, C and O elements in $Co_{1/2}Ni_{1/2}$-HIPA disperse evenly (Fig. 2c).

As shown in Fig. 3a, the linear sweep voltammetry (LSV) tests were applied to evaluate OER performances of Co_xNi_{1-x}-HIPA at 25 °C. Co-HIPA shows an overpotential of 412 mV when the current density reaches 10 mA/cm^2. Ni-HIPA basically manifests no OER behavior throughout the working potential range. The overpotential of Co_xNi_{1-x}-HIPA varies with the content of Co/Ni centers at 10 mA/cm^2: 380 mV for $Co_{4/5}Ni_{1/5}$-HIPA, 386 mV for $Co_{2/3}Ni_{1/3}$-HIPA and 432 mV for $Co_{1/3}Ni_{2/3}$-HIPA. It is noted that a minimum overpotential of 367 mV at 10 mA/cm^2 can be achieved by the optimal $Co_{1/2}Ni_{1/2}$-HIPA. Based on LSV curves, TS were calcu-

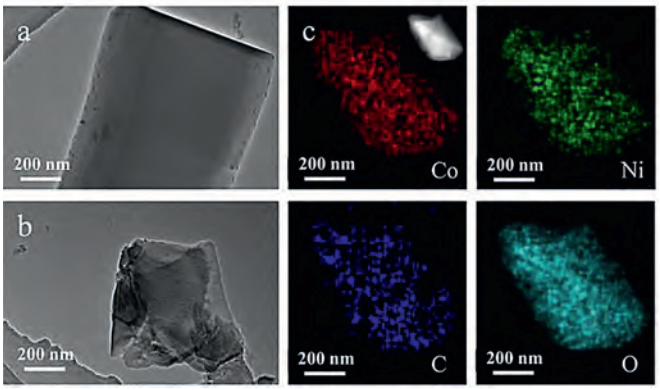

Fig. 2. TEM images (a, b), STEM image and EDS elemental mappings (c) of $Co_{1/2}Ni_{1/2}$-HIPA.

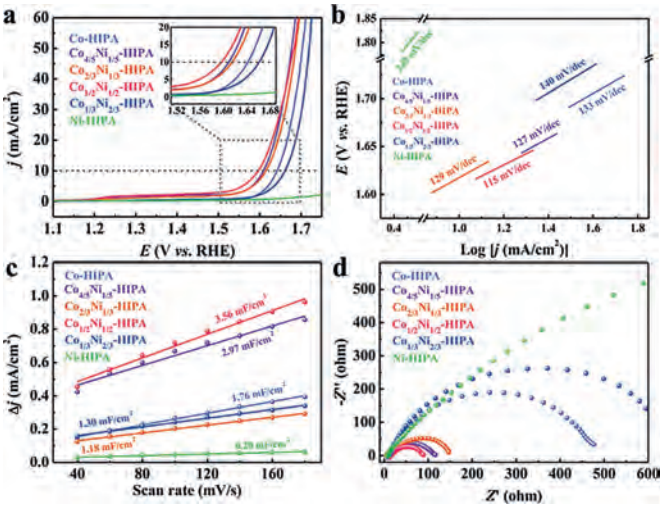

Fig. 3. LSV curves (a), Tafel plots (b), C_{dl} (c) and EIS (d) of Co_xNi_{1-x}-HIPA (x = 0, 1/3, 1/2, 2/3, 4/5, 1) at 25 °C.

lated to explore the intrinsic reaction kinetics (Fig. 3b). Ni-HIPA delivers the highest TS (349 mV/dec), which is consistent with its poor OER activity. Co-HIPA shows a TS of 133 mV/dec. Besides $Co_{1/3}Ni_{2/3}$-HIPA (140 mV/dec), the TS of the other bimetallic catalysts all decreased compared to the monometallic counterparts. $Co_{1/2}Ni_{1/2}$-HIPA has the lowest TS of 115 mV/dec. Further-

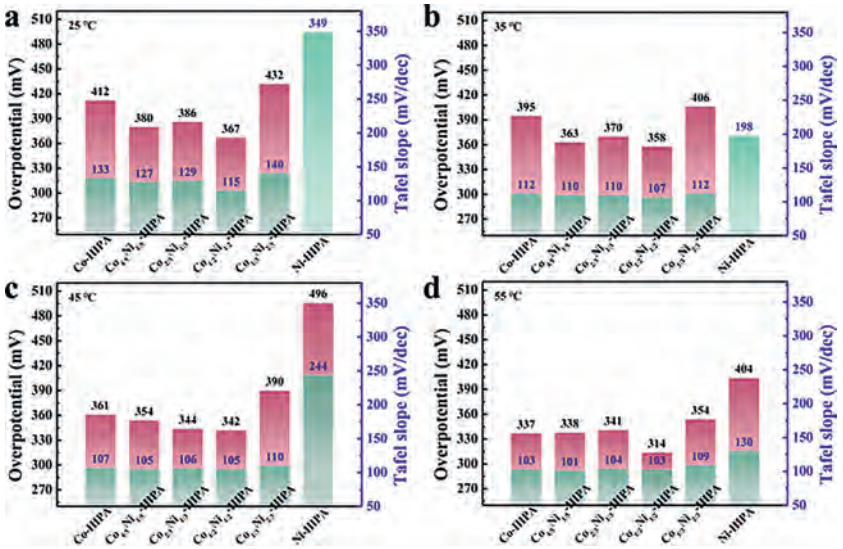

Fig. 4. Comparison of the overpotentials at 10 mA/cm^2 (left axis) and TS (right axis) of Co_xNi_{1-x}-HIPA (x = 0, 1/3, 1/2, 2/3, 4/5, 1) at 25 °C (a), 35 °C (b), 45 °C (c), 55 °C (d).

more, the electrochemically active surface areas (ECSAs) of the catalysts were evaluated by means of double-layer capacitances (C_{dl}), which were calculated from non-faradaic cyclic voltammograms (CV) measurements (Fig. 3c and Fig. S4 in Supporting information). $Co_{1/2}Ni_{1/2}$-HIPA has a C_{dl} of 3.56 mF/cm^2, which distinctly exceeds that of Co-HIPA (1.76 mF/cm^2), Ni-HIPA (0.20 mF/cm^2) and other bimetallic Co_xNi_{1-x}-HIPA, and demonstrates more electroactive sites exposed on the catalyst surface [39]. The Nyquist plots radius of $Co_{1/2}Ni_{1/2}$-HIPA is significantly smaller than those of other Co_xNi_{1-x}-HIPA. This smaller charge transfer resistance of $Co_{1/2}Ni_{1/2}$-HIPA is conducive to improve the catalytic performance (Fig. 3d). A high Faradaic efficiency of 96.2% for $Co_{1/2}Ni_{1/2}$-HIPA was able to be reached based on an average ring current of 57.7 μA (Fig. S5 in Supporting information).

$Co_{1/2}Ni_{1/2}$-HIPA exhibited durability over 16 h through the chronoamperometry test (Fig. S6 in Supporting information), demonstrating itself to be a promising competitor among other reported CP-based catalysts (Table S2 in Supporting information). The overpotential of $Co_{1/2}Ni_{1/2}$-HIPA at 10 mA/cm^2 increased 49 mV after 16 h chronoamperometric test, while the overpotential at 100 mA/cm^2 increased merely 10 mV (Fig. S7a in Supporting information). After 1000 CV cycles, the overpotential of $Co_{1/2}Ni_{1/2}$-HIPA at 10 mA/cm^2 increased by 56 mV, while the overpotential at 100 mA/cm^2 was almost identical to the initial value (Fig. S7b in Supporting information), indicating the excellent durability of $Co_{1/2}Ni_{1/2}$-HIPA. The morphology of $Co_{1/2}Ni_{1/2}$-HIPA after the chronoamperometry test was examined by SEM (Fig. S8 in Supporting information). The regular rod-like structure basically remains unchanged. According to EDS test, the molar ratio of Co and Ni in $Co_{1/2}Ni_{1/2}$-HIPA increased slightly (Table S3 in Supporting information), which may be one of the causes leading to the degradation of the catalyst performance.

Furthermore, the effect of temperature on the catalytic activity of OER was also studied. The LSV curves and Tafel plots of Co_xNi_{1-x}-HIPA at 35–55 °C are shown in Supporting information Fig. S9. The overpotential at 10 mA/cm^2 and the TS of Co_xNi_{1-x}-HIPA decrease evidently as the temperature increases, indicating the enhanced activities at increased temperatures (Fig. 4). In particular, Ni-HIPA exhibits a significant promotion of OER performance where the overpotential at 10 mA/cm^2 reaches 404 mV along with a TS of 130 mV/dec at 55 °C. The optimal $Co_{1/2}Ni_{1/2}$-HIPA continuously delivers the smallest overpotential and the lowest TS throughout all selected temperatures, in which the lowest overpotential of 314 mV at 10 mA/cm^2 and TS of 103 mV/dec are obtained at 55 °C. All Co_xNi_{1-x}-HIPA exhibit enhanced turnover frequency (TOF) compared to Co/Ni-HIPA at 380 mV (Table S4 in Supporting information). $Co_{1/2}Ni_{1/2}$-HIPA possesses the highest TOF of 0.025 s^{-1} at 25 °C and 0.074 s^{-1} at 55 °C. Based on the CV curves at different scan rates (Figs. S10-S12 in Supporting information), the ECSAs of Co_xNi_{1-x}-HIPA were calculated (Figs. S13a–c in Supporting information). The C_{dl} of $Co_{1/2}Ni_{1/2}$-HIPA remains higher than those of other catalysts at elevated temperatures, corresponding to more active sites on the catalyst surface. The electrochemical impedance spectroscopy (EIS) tests of Co_xNi_{1-x}-HIPA show that $Co_{1/2}Ni_{1/2}$-HIPA has a smaller charge transfer resistance at all selected temperatures (Figs. S13d-f in Supporting information).

In order to understand the different activities of Co_xNi_{1-x}-HIPA, the activation energies based on the charge transfer resistance at different temperatures were calculated. The Nyquist plots radii of Co_xNi_{1-x}-HIPA were reduced at increased temperature (Fig. S14 in Supporting information). The equivalent circuit of the impedance curve is given in Fig. S15 (Supporting information), where R_s represents the resistance of the electrolyte, CPE represents the constant phase element, and R_{ct} represents the charge transfer impedance. The exchange current (i_0) and apparent activation energy (E_a) of the electrode are calculated by the following Eqs. 1 and 2 [40,41]:

$$i_0 = RT/nFR_{ct} \quad (1)$$

$$i_0 = A\exp(-E_a/RT) \quad (2)$$

where A is a coefficient independent of temperature, R is gas constant, T is absolute temperature, n is the number of electrons transferred, and F is Faraday constant. The R_{ct} and i_0 values of Co_xNi_{1-x}-HIPA at different temperatures are given in Supporting information Table S5. i_0 represents the difficulty when the catalyst gains and loses electrons at reaction equilibrium state, which means how easily the catalytic reaction occurs. $Co_{1/2}Ni_{1/2}$-HIPA has the smallest R_{ct} and i_0 at all selected temperatures, corresponding to the highest catalytic activity. Arrhenius plots show that $Co_{1/2}Ni_{1/2}$-HIPA has the lowest activation energy of 19.91 kJ/mol and in consequence, the best OER performance of this family (Fig. 5).

XPS surveys were conducted to examine the electronic states of different metal centers. Co, Ni, C and O elements coexist in all Co_xNi_{1-x}-HIPA (Fig. S16 in Supporting information). To obtain

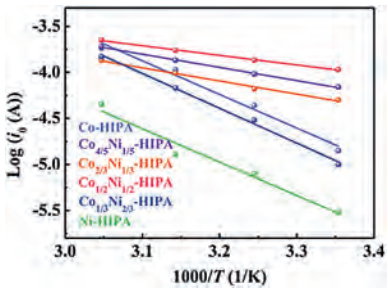

Fig. 5. Arrhenius plots of Log i_0 *vs.* $1/T$ of Co_xNi_{1-x}-HIPA (x = 0, 1/3, 1/2, 2/3, 4/5, 1).

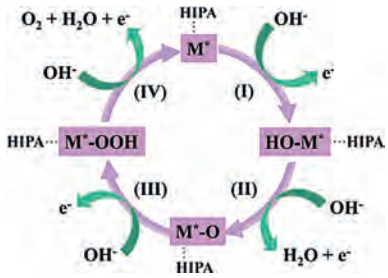

Fig. 6. Proposed OER mechanism on Co_xNi_{1-x}-HIPA (x = 0, 1/3, 1/2, 2/3, 4/5, 1) in alkaline medium (M* represented for Co and Ni centers).

more detailed information of the surface electronic states, the corresponding high-resolution XPS of all samples have been measured (Fig. S17 in Supporting information). The binding energies of Co $2p_{3/2}$ and Co $2p_{1/2}$ in Co-HIPA are 779.1 eV and 794.7 eV [42,43], while the binding energies of Ni $2p_{3/2}$ and Ni $2p_{1/2}$ in Ni-HIPA are located at 853.5 eV and 871.2 eV [32,44]. Compared with Co-HIPA and Ni-HIPA, the binding energies of Co $2p_{3/2}$ and Co $2p_{1/2}$ of all bimetallic CPs slightly downshift, while the binding energies of Ni $2p_{3/2}$ and Ni $2p_{1/2}$ slightly upshift (Table S6 in Supporting information). This variation of binding energy is ascribed to the increased electron density of Co center and the decreased electron density of Ni center [45]. Through the mixed-metal strategy, the simultaneous introduction of Co and Ni with different ratios was able to alter electronic states, thus influencing the formation of active intermediates during the catalytic process [45,46]. According to literatures, M*OOH is a common water oxidation active intermediate in alkaline electrolyte, which is generated by continuous attacks of OH^- on M* and serves as a crucial intermediate for oxidation of OH^-. The increase in the electron density of the Co centers in CPs is conducive to the improvement of OER electrocatalytic performance [47–50]. Based on the above analysis, an OER mechanism is presented in Fig. 6.

To further confirm the origin of the $Co_{1/2}Ni_{1/2}$-HIPA as highly efficient electrocatalyst, the change of composition and electron state after 16 h chronoamperometry test were studied by XPS spectra. After chronoamperometry test, the binding energy of Co 2p (778.8 eV for Co $2p_{3/2}$) and Ni 2p (852.9 eV for Ni $2p_{3/2}$) downshift compared to that of pristine $Co_{1/2}Ni_{1/2}$-HIPA (Fig. S18 in Supporting information). This phenomenon could be attributed to the formation of intermediate of $M(OH)_2$ during OER process [49]. The new peak emerged at the binding energies of 777.0 eV can be attributed to Co^{3+}, which was consistent with the proposed mechanism [51,52]. As revealed by FTIR results (Fig. S19 in Supporting information), the main peaks of the title compounds after OER are almost unchanged compared to that of the compounds before OER. The peaks located at 1621 cm^{-1} and 1354 cm^{-1} are assigned to asymmetric and symmetric stretching vibrations of −COOH [53]. On the basis of the above analysis, it can be deduced that M*OOH and $M(OH)_2$ surrounding with the HIPA ligands emerged as the reaction proceeded, of which M*OOH acted as the active site.

To summarize, a mixed-metal strategy is proposed to synthesize a series of bimetallic cobalt-nickel coordination polymers as electrocatalysts for oxygen evolution reaction. The optimal $Co_{1/2}Ni_{1/2}$-HIPA exhibits an overpotential of 367 mV at 10 mA/cm^2 with reduced charge transfer resistance and enhanced active surface area compared to single-metal CPs. The optimized $Co_{1/2}Ni_{1/2}$-HIPA also shows the lowest overpotential at 10 mA/cm^2 throughout all selected temperatures and possesses minimum activation energy. This work provides a powerful and facile way to simultaneously optimize the composition and the electron states for enhancing catalytic performance of CP-based electrocatalysts.

Declaration of competing interest

The authors declare that they have no known competing financial interests or personal relationships that could have appeared to influence the work reported in this paper.

Acknowledgments

This work was supported by the National Natural Science Foundation of China (Nos. 21622105 and 21931004), the Natural Science Foundation of Tianjin (No. 18JCJQJC47200), and the Ministry of Education of China (No. B12015).

Appendix A. Supplementary data

Supplementary material associated with this article can be found, in the online version, at doi:10.1016/j.cclet.2021.10.090.

References

[1] T. Hisatomi, K. Domen, Nat. Catal. 2 (2019) 387–399.
[2] C.L. Hu, L. Zhang, J.L. Gong, Energy Environ. Sci. 12 (2019) 2620–2645.
[3] W. Wang, X.M. Xu, W. Zhou, Z.P. Shao, Adv. Sci. 4 (2017) 1600371.
[4] M. Kim, J. Park, M. Kang, J.Y. Kim, S.W. Lee, ACS Cent. Sci. 6 (2020) 880–891.
[5] N.T. Suen, S.F. Hung, Q. Quan, N. Zhang, Y.J. Xu, H.M. Chen, Chem. Soc. Rev. 46 (2017) 337–365.
[6] J. Du, F. Li, L.C. Sun, Chem. Soc. Rev. 50 (2021) 2663–2695.
[7] B. You, Y.J. Sun, Acc. Chem. Res. 51 (2018) 1571–1580.
[8] Z.P. Wu, X.F. Lu, S.Q. Zang, X.W.D. Lou, Adv. Funct. Mater. 30 (2020) 1910274.
[9] F.L. Lyu, Q.F. Wang, S.M. Choi, Y.D. Yin, Small 15 (2019) 1804201.
[10] Z.P. Shi, X. Wang, J.J. Ge, C.P. Liu, W. Xing, Nanoscale 12 (2020) 13249–13275.
[11] Q.R. Shi, S.F. Fu, Z.C. Zhu, J.H. Song, D. Du, Y.H. Lin, Mater. Horiz. 6 (2019) 684–702.
[12] K. Fan, H.Y. Zou, Y. Lu, et al., ACS Nano 12 (2018) 12369–12379.
[13] K. Jiang, M. Luo, M. Peng, et al., Nat. Commun. 11 (2020) 2701.
[14] T. Reier, H.N. Nong, D. Teschner, R. Schlögl, P. Strasser, Adv. Energy Mater. 7 (2017) 1601275.
[15] C.L. Hu, L. Zhang, J.L. Gong, Energy Environ. Sci. 12 (2019) 2620–2645.
[16] K.A. Stoerzinger, R.R. Rao, X.R. Wang, et al., Chem 2 (2017) 668–675.
[17] C.T. Hsieh, C.L. Huang, Y.A. Chen, S.Y. Lu, Appl. Catal. B: Environ. 267 (2020) 118376.
[18] S.L. Zhao, C.H. Tan, C.T. He, et al., Nat. Energy 5 (2020) 881–890.
[19] W.R. Cheng, X. Zhao, H. Su, et al., Nat. Energy 5 (2019) 115–122.
[20] J. Perego, I. Villa, A. Pedrini, et al., Nat. Photonics 15 (2021) 393–400.
[21] Z.H. Chen, Z.S. Han, W. Shi, P. Cheng, Acta Chim. Sin. 78 (2020) 1336–1348.
[22] S.Y. Bai, B. Kim, C. Kim, et al., Nat. Nanotechnol. 16 (2021) 77–84.
[23] L.L. Lu, B.Y. Wu, W. Shi, P. Cheng, Inorg. Chem. Front. 6 (2019) 3456–3467.
[24] R.Z. Zhang, B.Y. Wu, Q. Li, L.L. Lu, W. Shi, P. Cheng, Coord. Chem. Rev. 422 (2020) 213436.
[25] S.Y. Zhang, Z.Y. Wang, J. Gao, et al., Chem 5 (2019) 1609–1618.
[26] Y.H. Wang, Q. Li, W. Shi, P. Cheng, Chin. Chem. Lett. 31 (2020) 1768–1772.
[27] H.J. Xu, Y.W. Yang, X.X. Yang, et al., J. Mater. Chem. A 7 (2019) 8284–8291.
[28] X. Wang, L.L. Chai, J.Y. Ding, et al., Nano Energy 62 (2019) 745–753.
[29] Z.Q. Xue, K. Liu, Q.L. Liu, et al., Nat. Commun. 10 (2019) 5048.
[30] W.L. Li, F.S. Li, H. Yang, et al., Nat. Commun. 10 (2019) 5074.
[31] K. Rui, G.Q. Zhao, Y.Q. Chen, et al., Adv. Funct. Mater. 28 (2018) 1801554.
[32] Q. Li, L.L. Lu, J.W. Liu, W. Shi, P. Cheng, J. Energy Chem. 63 (2021) 230–238.
[33] F.L. Li, P.T. Wang, X.Q. Huang, et al., Angew. Chem. Int. Ed. 58 (2019) 7051–7056.
[34] X.R. Zheng, Y.H. Cao, D.Y. Liu, et al., ACS Appl. Mater. Interfaces 11 (2019) 15662–15669.
[35] W.X. Li, W. Fang, C. Wu, et al., J. Mater. Chem. A 8 (2020) 3658–3666.

[36] D.J. Li, Q.H. Li, Z.G. Gu, J. Zhang, J. Mater. Chem. A 7 (2019) 18519–18528.
[37] X. Zhao, B. Pattengale, D. Fan, et al., ACS Energy Lett. 3 (2018) 2520–2526.
[38] J. Du, J. Ren, M. Shu, et al., Angew. Chem. Int. Ed. 60 (2021) 4142–4149.
[39] X. Zhang, Y.F. Zhao, Y.X. Zhao, et al., Adv. Energy Mater. 9 (2019) 1900881.
[40] H. Ma, S.Y. Zhang, W.Q. Ji, Z.L. Tao, J. Chen, J. Am. Chem. Soc. 130 (2008) 5361–5367.
[41] W.C. Hu, Y. Shi, Y. Zhou, et al., J. Mater. Chem. A 7 (2019) 10601–10609.
[42] Y. Yamada, K. Yano, Q. Xu, S. Fukuzumi, J. Phys. Chem. C 114 (2010) 16456–16462.
[43] W.L. Ding, Y.H. Cao, H. Liu, et al., Rare Met. 40 (2021) 1373–1382.
[44] W. Zhou, D.D. Huang, Y.P. Wu, et al., Angew. Chem. Int. Ed. 58 (2019) 4227–4231.
[45] T. Reier, Z. Pawolek, S. Cherevko, et al., J. Am. Chem. Soc. 137 (2015) 13031–13040.
[46] H. Dong, X. Zhang, X.C. Yan, et al., ACS Appl. Mater. Interfaces 11 (2019) 45080–45086.
[47] M.S. Wu, G.W. Lin, R.S. Yang, J. Power Sources 272 (2014) 711–718.
[48] B.S. Yeo, A.T. Bell, J. Am. Chem. Soc. 133 (2011) 5587–5593.
[49] X.H. Zhao, B. Pattengale, D.H. Fan, et al., ACS Energy Lett. 3 (2018) 2520–2526.
[50] D.S. Raja, C.L. Huang, Y.A. Chen, Y.M. Choi, S.Y. Lu, Appl. Catal. B: Environ. 279 (2020) 119375.
[51] Y. Lu, D.Q. Fan, Z.P. Chen, et al., Sci. Bull. 65 (2020) 460–466.
[52] X.D. Jia, X. Zhang, J.Q. Zhao, et al., J. Energy Chem. 34 (2019) 57–63.
[53] M. Armand, S. Grugeon, H. Vezin, et al., Nat. Mater. 8 (2009) 120–125.